

KEK-preprint-95-139

## Recent results from TRISTAN\*

Ryoji Enomoto<sup>†</sup>

*National Laboratory for High Energy Physics, KEK  
1-1 Oho, Tsukuba-city, Ibaraki 305, Japan.*

*Representing the TRISTAN Experiments*

**Abstract**

The TRISTAN results from 1994 to 1995 are reviewed in this report. The physics results dominated the  $\gamma\gamma$  physics. Therefore, only these are selected in this article. We have systematically investigated jet productions, the  $\gamma$ -structure function, and charm pair productions in  $\gamma\gamma$  processes. The results, discussions, and future prospects are presented.

**1 TRISTAN**

Initially, the TRISTAN project was aimed at finding the “top” quark [1]. Although only a three-km circumference was available, we achieved a maximum beam energy of 33 GeV. Unfortunately, the top mass was far beyond this energy [2]. We, thus, converted our target to a high-luminosity operation of this collider. Figure 1 shows the relationship between the beam energies and luminosities for various accelerators. Assuming that CLEO and LEP are standard, we can see why TRISTAN is a high-luminosity machine. We hope that the same thing occurs in the near-future B-factory [3]. As a matter of fact, we (TOPAZ, VENUS, and AMY) obtained  $\int L dt$  of  $300\text{pb}^{-1}$  per each experiment at  $\sqrt{s}=58$  GeV.

If there is a process having a cross section that is an increasing function of  $\sqrt{s}$ , that may be a big target until the B-factory starts.  $\gamma\gamma$  physics is one of them. The luminosity function ( $L_{\gamma\gamma}$ ) is roughly proportional to  $\log(s)$ . As a result, TRISTAN becomes the highest luminosity  $\gamma\gamma$ -factory, except for the low  $W_{\gamma\gamma}$  region, where CESR still gives the highest  $\gamma\gamma$  yield. Therefore, CESR has been fitted for resonance physics, and TRISTAN is for parton physics. For a higher  $W_{\gamma\gamma}$  region ( $> 6$  GeV), we have obtained the largest statistics; this situation will remain forever. TRISTAN can play an important role in particle physics, especially regarding strong interactions.

---

\* Talk presented at SLAC Summer Institute, Topical Conf. 1995.

<sup>†</sup> Internet address: enomoto@bsun03.kek.jp.

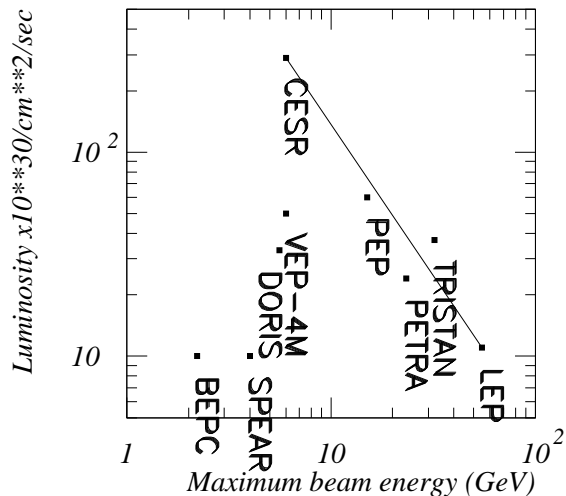


Figure 1: Luminosities versus the maximum beam energies of various  $e^+e^-$  colliders.

## 2 $\gamma\gamma$ Physics

Here, we briefly mention the  $\gamma\gamma$  processes. Figure 2 shows four typical diagrams which contribute to these. (a) is called a “direct process”, where photons interact with quarks via point-like interactions [4]. The vector-meson dominance process (VDM) is shown in (b) [5]. (c) and (d) are called the “resolved-photon process”, where partons inside photons interact point-like [6]. (a) contributes to high- $P_T$  production of quarks, (b) to a low  $P_T$ , and (c), (d) to a medium  $P_T$ . Considering our sensitivity over the  $W_{\gamma\gamma}$  range, in addition to our trigger system ability [7], we can study (a), (c), and (d) at most accurate levels.

To conclude, we are sensitive for  $\gamma$ -structure studies, especially concerning the partonic structure of the photon, in addition to higher order of QCD (or strong interaction). The most important topic is to determine the gluonic densities inside photons. This is the cleanest way to determine the  $\gamma$ -structure in contrast with ep collisions at HERA experiments.

## 3 Detector

Three groups (TOPAZ, VENUS, and AMY) were operating at TRISTAN. Among them, we pay special attention to the TOPAZ experiments, because of having low-angle calorimeters.

The apparatus of the TOPAZ detector is shown in Figure 3 [8]. The central tracker is a TPC, which enables us to study heavy flavor productions. TOPAZ is the only detector having low-angle calorimeters (FCL)[9]. This covers a polar angle region from 3.2 to 12 degrees with respect to the beam axis. The mean beam energy( $E_b$ ) of TRISTAN was 29

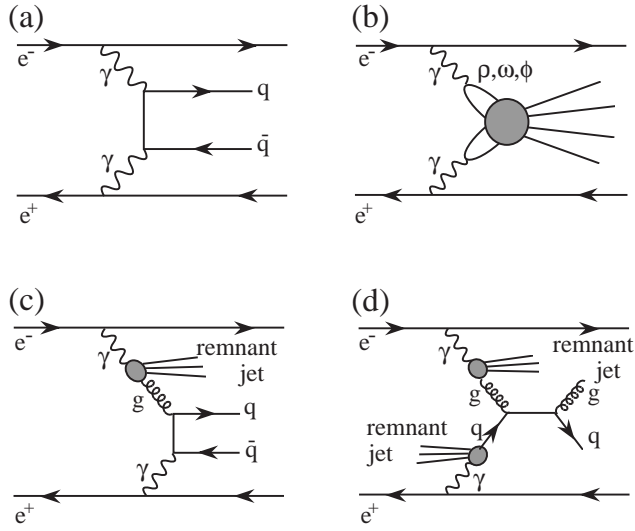


Figure 2: Feynman diagrams which contributed to  $\gamma\gamma$  processes at TRISTAN.

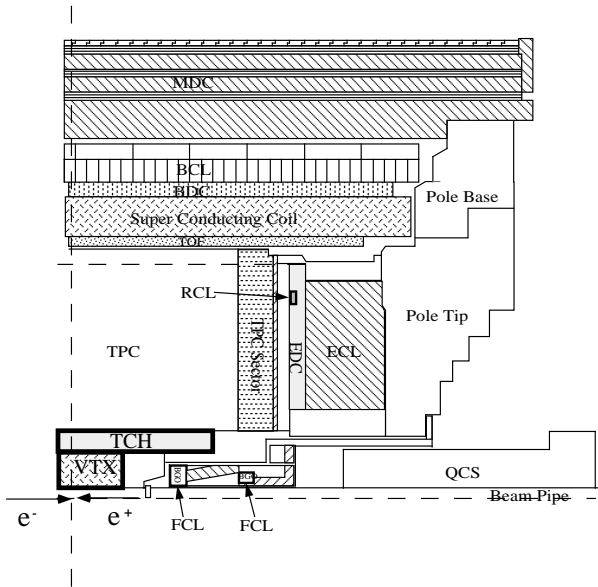


Figure 3: TOPAZ detector

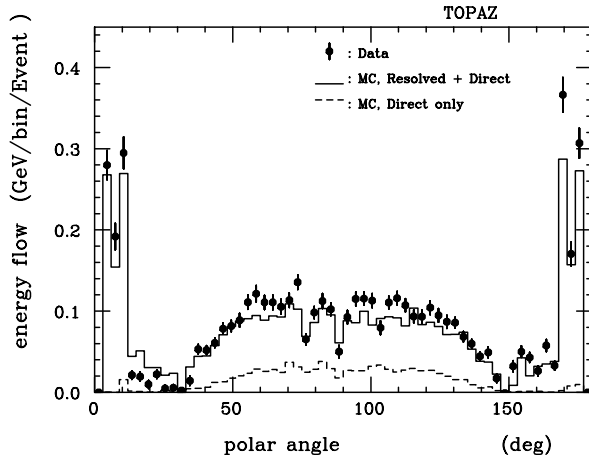


Figure 4: Energy flow of  $\gamma\gamma \rightarrow 2jets$  events. The histograms are the Monte-Carlo prediction; the dashed one is the direct process and the solid one is the resolved and direct process.

GeV. When we select events with an energy deposit of  $0.4E_b$  (beam-electron tag), the  $Q^2$  for the photon is greater than  $1.05 \text{ GeV}^2$ .

In addition to the beam-electron tag, we have introduced a “remnant-jet-tag”. As shown in Figures 2 (c) and (d), hadron jets which are resolved from photons flow into beam directions. Typically, hadrons from these jets have  $P_T$ ’s of about 0.4 GeV. Assuming that these hadrons have energies of several GeV, they hit the FCL fiducial region. The energy flow in typical  $\gamma\gamma \rightarrow 2jets$  events are shown in Figure 4. It has enhancements at low-angle regions which cannot be explained by the processes shown in Figures 2 (a) nor (b).

The energy deposits in the FCL are also shown in Figure 5. The soft component corresponds to these resolved-photon events. We can, therefore, tag the resolved-photon process by selecting a soft energy deposit in the FCL. The efficiency of this tagging was estimated to be  $\sim 80\%$  with a background of 10%, mostly due to the beam background. We call this “remnant-jet-tag”, or “rem-tag” in short.

## 4 Event Structure

### 4.1 Event Shapes

As has been described, various processes contribute to  $\gamma\gamma$  collisions; the analysis ways are not unique. According to a historical method, hadron system at the CMS frame were divided into two hemispheres (definition of jets). This method has an advantage for

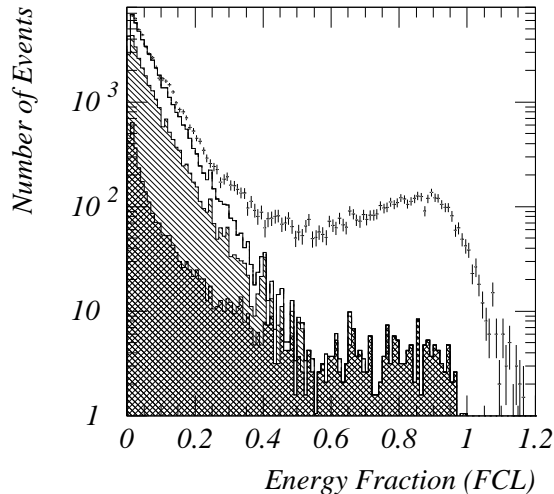


Figure 5: Distribution of the energy fractions (normalized at the beam energy) of the maximum-energy clusters in FCL. The points with error bars are experimental data. The histograms are predictions by a Monte-Carlo simulation; the cross-hatched area is a single-photon-exchange process, the singly-hatched one is VDM, and the open one is a resolved-photon process.

analyzing events in all  $P_T$  regions. AMY showed evidence for a resolved-photon process by this method [10]. A similar analysis was carried out by TOPAZ, and the  $P_T^{jet}$  distribution is shown in Figure 6 (a). For example, at  $P_T^{jet}=2.5$  GeV, the data excess is by a factor of 2.5 compared with the incoherent sum of direct and VDM processes. This excess has been explained by the resolved-photon process. Next, the thrust distribution of high  $P_T^{jet}$  ( $>2.5$  GeV) events are plotted in Figure 6 (b). The events are spherical, consistent with the prediction by the resolved-photon processes. Similar results have been obtained by the LEP experiments [11, 12].

## 4.2 Jet Cross Section

The processes shown in Figures 2 (a), (c), and (d) include hard scattering of partons which are observed as jets (Figure 7). These jets are reconstructed in  $\phi$  and  $\eta$  plane. The particles within the circle  $R = \sqrt{(\phi - \phi_0)^2 + (\eta - \eta_0)^2}$  are used. Figure 8 is the cross section of jet production versus  $P_T^{jet}$ . The cross section is consistent with the incoherent sum of the direct and resolved-photon processes at the  $P_T^{jet} > 2\text{GeV}$  region (the same result as the previous one). The theoretical models, called LAC1, LAC3, and DG, shown in the Figure have significant differences in the gluon distribution inside the photon [13, 14]. The hard-gluon model (LAC3) is clearly rejected. LAC1 and DG show difference at low-x gluonic-density, and it is difficult to distinguish them by this experimental method [15].

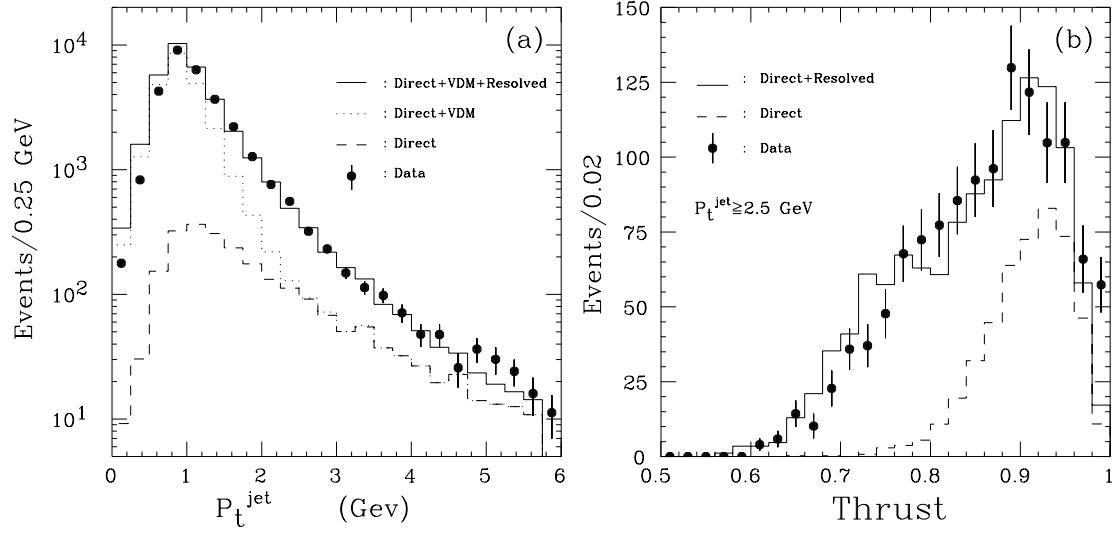


Figure 6: (a)  $P_T^{jet}$  distribution. The histograms are theoretical predictions; the dashed one is a direct process, the dotted one is the direct and VDM, and the solid one is the sum of these two and the resolved-photon process. (b) Thrust distribution of high  $P_T^{jet}$  ( $> 2.5$  GeV) events.

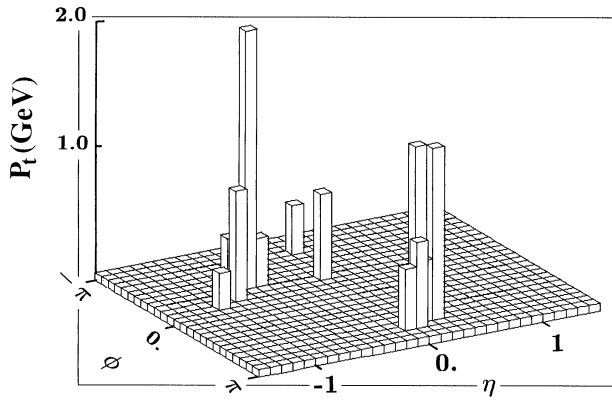


Figure 7: Typical jets observed by the TOPAZ detector.

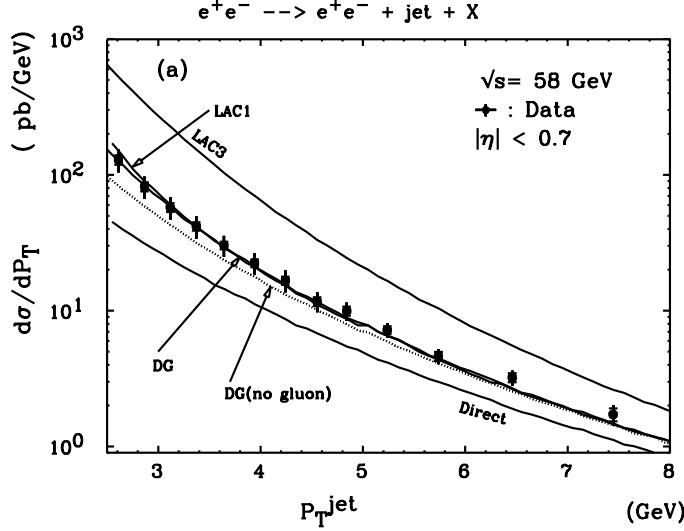


Figure 8: Jet production cross section in  $\gamma\gamma$  collisions.

A similar result was obtained by AMY [16].

## 5 Structure Function

The photon structure function ( $F_2^\gamma$ ) was measured by the TOPAZ collaboration [17]. We obtained a high value compared with the theoretical values at  $x \sim 0.04$  at  $3 < Q^2 < 30$   $\text{GeV}^2$ . These regions are important for determining the QCD-based models. Although the experimental ambiguities in determining  $x$  value from the mass of the measured hadronic system were found to be large, and there will be a systematic shift. We are, therefore, going to reanalyse the data using a new algorithm to determine  $x$  while assuming missing-energy flow directions (i.e., beam-pipe direction).

## 6 Charm Pair Production

According to a QCD calculation of parton-parton scattering, the cut-off parameter ( $P_T^{min}$ ) was introduced for light-quark scattering. This parameter must be determined experimentally; the optimum value was obtained to be around 1.7~2 GeV. Fortunately, for the charm-quark case, this parameter is not necessary, and we can experimentally select charm-pair events with high purity. In addition, the VDM effects are considered to be small for charmed-particle production. In the resolved-photon processes we only have to consider gluon-gluon scattering; therefore, this is sensitive to the gluonic density in which a large model dependence exists. The NLO calculations are available at the parton level [18].

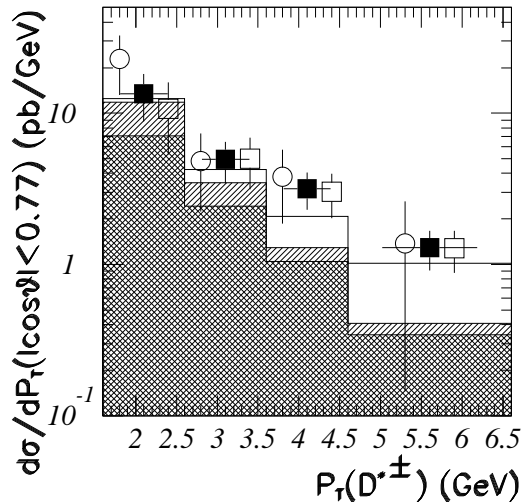


Figure 9: Differential cross sections of  $D^{*\pm}$  versus  $P_T$ . The open circles were obtained by the full reconstruction method, the open squares by the softpion method, and the closed squares are the average by these two methods. The histograms are the theoretical predictions: the cross hatched is the direct process, the singly hatched is the resolved, and the open area is obtained assuming the hypothetical  $\tilde{t}$  pair production.

## 6.1 Full and partial Reconstruction of $D^{*\pm}$

Initial charm quark fragment to  $D$  mesons.  $D^*$  is the most probable state. This fragmentation function is experimentally well known. We can, therefore, estimate the initial charm quarks'  $P_T$ s.

We first tried to reconstruct  $D^{*+} \rightarrow \pi_s^+ D^0 (D^0 \rightarrow K^- \pi^+ X)$  [19].  $20 \pm 5$   $D^*$ s were reconstructed with a good S/N ratio. The obtained cross section is plotted in Figure 9 by open circles. Although this cross section is higher than the sum of the direct and resolved-photon predictions, the statistics are low. The NLO effect was taken into account in the prediction. We used LAC1 for the gluonic density in photons.

In order to improve the experimental accuracy, we carried out a “softpion analysis” in reconstructing the  $D^*$ s. The results are also shown in Figure 9 by the open circles. They are consistent with that of the full reconstruction. The high  $P_T$  anomaly still existed, and the hypothetical  $\tilde{t}$  pair assumption was tested by looking at the event shapes [20]. These shapes differ from  $\tilde{t}$ -pair prediction and rather resemble the typical  $\gamma\gamma$  events. The similar high  $P_T$  anomaly was also reported by the AMY collaboration [21].

## 6.2 $K_s$ Inclusive

The maximum integrated luminosity of the TRISTAN experiment is  $300\text{pb}^{-1}$  and now most of them were analyzed. We must, therefore, seek other ways of analysis than waiting



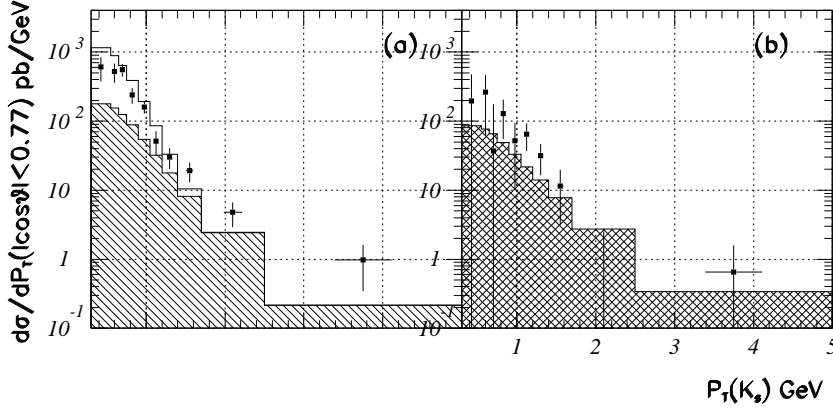


Figure 10: Differential cross sections of  $K_0$  versus  $P_T$ : (a) for the VDM and resolved-photon process, and (b) for the direct process. The histograms are the theoretical predictions; the definition of the hatches are as same as those for the previous figure.

for an increase in data. An inclusive analysis of the strange particle is one of them. The  $P_T$  spectrum of these reflect that of charm quarks. Also, strange-quark pair production is strongly suppressed in  $\gamma\gamma$  collisions.

In the  $K_s$  inclusive analysis, we introduced “remnant-jet-tag” [22]. The details were described in the previous section. We can, therefore, derive the cross sections process by process. These are shown in Figures 10 (a) and (b). Here, we could not separate the VDM and the resolved-photon events, because of the low- $P_T$  particle production by the VDM.

By this study, the existing theory plus the LAC1 parametrization with the NLO correction well describe the experimental data. We further tested the parametrization difference in the gluon density by using the WHIT parameterization [23]. This gave six systematic parametrizations. Some combinations of these with various  $P_T^{min}$  cut-offs, fitted the experimental data perfectly.

### 6.3 Electron Inclusive

The electron inclusive method is a cleaner one than the inclusive  $K_0$ . Here, we do not have to consider the VDM. The TOPAZ detector can identify very low  $P_T$  electrons, such as 0.4 GeV [24]. We can, therefore, measure the gluon density at very low- $x$  ( $\sim 0.02$ ), where the model differences appears. Figure 11 (a) is the differential cross section versus the electron  $P_T$ s. The experimental data clearly favor the LAC1 parametrization, also suggesting the necessity of the NLO correction and a low charm-quark mass of  $\sim 1.3$  GeV

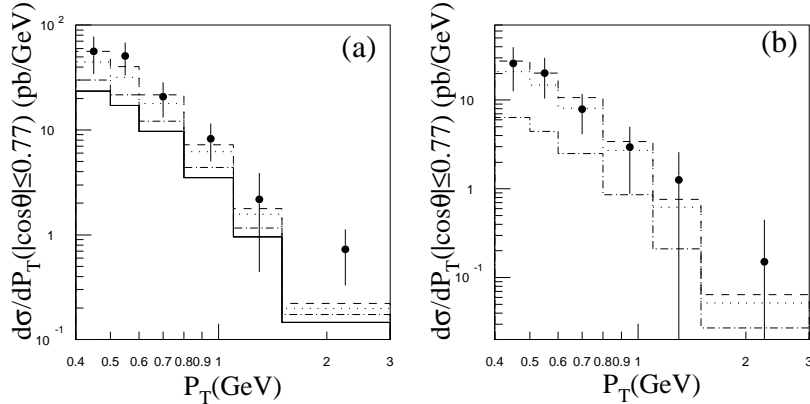


Figure 11: (a) Electron inclusive cross sections; the solid line is the direct process, the dot-dashed is the DG case, the dotted is the LAC1 with  $m_c=1.5$  GeV, and the dashed is the LAC1 with  $m_c=1.3$  GeV. (b) The resolved-photon cross section; the definition of lines are as same as (a).

[25]. Although VENUS produced a similar result, the statistics were about half that of ours [26].

We carried out “remnant-jet-tag”, and obtained purely “resolved-photon” cross section (Figure 11 (b)). Again, it confirmed our parametrization of the theory. We also observed a large difference between the DG and LAC1. This is because this method is sensitive to very low- $x$  regions where the jet analysis could not resolve. Note that this method is more powerful than the single tag experiment ( $F_2^\gamma$ ) in determining the gluon density inside photons.

In figure 11 (a) at highest  $P_T$  region, there are some excesses compared with the existing theory. A similar high  $P_T$  excess was observed by AMY [21].

## 6.4 $\Lambda$ Inclusive

So far what we have learned is that there are some high  $P_T$  excess in charm production, and that the experimental results at low  $P_T$  agree with the existing theory with the NLO correction and high gluonic density at low  $x$ . We investigated the  $\Lambda$ -inclusive cross section in order to qualitatively study the NLO effects. As can also tag charm-pair events the same as in the  $K_0$  case.

In addition, there is an experimental fact that a gluon-jet produces more  $\Lambda$ s than does a quark jet [27]. Our experimental results are shown in Table 1 [28]. There are process-independent excesses compared with the prediction of the LO theories. The values are a

tag cond.	Experiment	Theory (LO)	Exp./Theory	subprocess
antitag	$43.3 \pm 8.3$	19.1	$2.26 \pm 0.43$	VDM+resolved+direct
rem-tag (-VDM)	$15.6 \pm 3.5$	6.0	$2.60 \pm 0.58$	resolved
rem-tag	$34.8 \pm 7.8$	17.3	$2.01 \pm 0.45$	VDM+resolved
anti-rem	$27.7 \pm 7.9$	13.1	$2.11 \pm 0.60$	VDM+direct

Table 1: Total cross section (pb) of  $\Lambda(\bar{\Lambda})$  in the  $|\cos\theta| < 0.77$  and  $0.75 < P_T < 2.75$  GeV range. The notation (-VDM) means VDM subtraction using theory. Here, we use the LO theories in order to show the discrepancy with the experimental data.

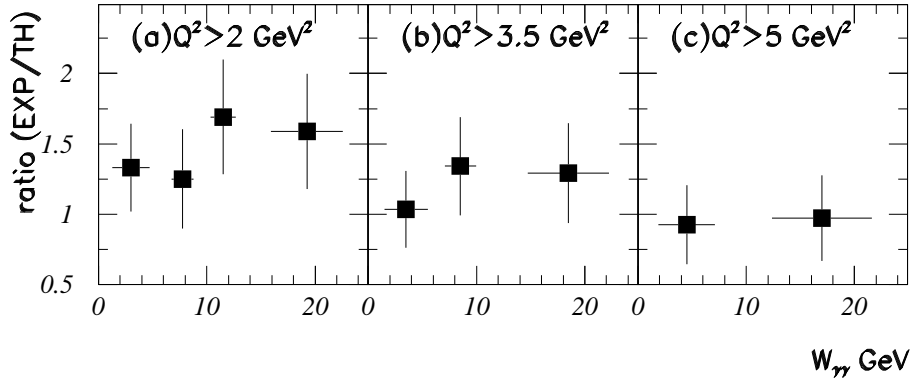


Figure 12: Ratios of the experimental and theoretical cross sections in various kinematic regions; (a)  $Q_{\gamma,min}^2 > 2\text{GeV}^2$ , (b)  $Q_{\gamma,min}^2 > 3.5\text{GeV}^2$ , and (c)  $Q_{\gamma,min}^2 > 5\text{GeV}^2$ . The  $Q_{\gamma,min}^2$  is specified in the text.

factor of two. We can, therefore, conclude that there exists significant gluon jet production in  $\gamma\gamma$  collisions, i.e., the NLO effect.

## 7 Double Tag

We carried out a double-tag analysis, and obtained the total hadronic cross sections [31]. The  $Q^2$  ranges for  $\gamma^*$  was  $2 \sim 25 \text{ GeV}^2$  and the  $W$  range was  $2 \sim 25 \text{ GeV}$ . Figure 12 is the ratio of the cross sections ( $e^+e^- \rightarrow e^+e^-h$ ) between the experiment and the LO  $e^+e^- \rightarrow e^+e^-q\bar{q}$  theory. The experimental value agrees with the LO prediction in the high- $Q^2$  region. There are enhancements of  $\sim 30\%$  in the low- $Q^2$  region, suggesting NLO effects.

## 8 Discussion

Our experimental data strongly favor a large gluon density at low  $x$ , as has been suggested by LAC1. However, the HERA experiment (ep collision) showed a lower gluon density than that which LAC1 predicted [29]. Also, the LEP experiment is inconsistent with LAC1 at low  $x$  [30]. The problem is whether we can explain all of the experimental data by simply changing the parton density functions. In addition, the high  $P_T$  excess in charm production can not be solved by any existing theories.

The cross section of the  $\gamma\gamma$  collision increases with energy in a future  $e^+e^-$  linear collider experiment. It would be a large background, and may be related to such physics as  $H \rightarrow \gamma\gamma$  searches. In order to reliably estimate the background, our measurement greatly helps. Systematic measurements, such as  $\gamma\gamma \rightarrow h^\pm X$  and  $\gamma X$ , are necessary.

## 9 Conclusion

At the TRISTAN  $e^+e^-$  collider, a systematic study of hadronic  $\gamma\gamma$  collisions was carried out. TRISTAN is a high-luminosity  $\gamma\gamma$  factory, and our data of these processes have the largest statistics. For parton production our data greatly contributed to our experimental and theoretical understanding of photon structures. Further systematic measurements on various processes are awaited.

## Acknowledgements

I thank to Drs. H. Hayashii, M. Iwasaki, and T. Nozaki for summarizing these results. I also thank to the TOPAZ collaboration and the KEK accelerator division.

## References

- [1] TRISTAN Project Group, KEK Report 86-14 (1987).
- [2] F. Abe et al., Phys. Rev. Lett. **74** (1995) 2626; A. Abachi et al., Phys. Rev. Lett. **74** (1995) 2632.
- [3] The BELLE collaboration, Letter of Intent, KEK Report 94-2 (1994).
- [4] B. J. Brodsky, T. Kinoshita, and H. Terazawa, Phys. Rev. **D4** (1971) 1532.
- [5] J. J. Sakurai, "Currents and mesons", Univ. of Chicago Press (1969).
- [6] S. J. Brodsky, T. A. DeGrand, J. F. Gunion, and J. H. Weis, Phys. Rev. Lett. **41** (1978) 672; H. Terazawa, J. Phys. Soc. Jpn. **47** (1979) 355.

- [7] R. Enomoto et al., Nucl. Instrum. Meth. **A269** (1988) 507; R. Enomoto, K. Tsukada, N. Ujiie, and A. Shirahashi, IEEE Trans. on NS. **35** (1988) 419; T. Tsukamoto, M. Yamauchi, and R. Enomoto, Nucl. Instrum. Meth. **A297** (1990) 148.
- [8] T. Kamae et al., Nucl. Instrum. Meth. **A252** (1986) 423; S. Kawabata et al., Nucl. Instrum. Meth. **A270** (1988) 11; J. Fujimoto et al., Nucl. Instrum. Meth. **A256** (1987) 449; A. Yamamoto et al., Jpn. J. Appl. Phys. Lett. **55** (1986) L440.
- [9] H. Hayashii et al., Nucl. Instrum. Meth. **A316** (1992) 202.
- [10] R. Tanaka et al., Phys. Lett. **B277** (1992) 215.
- [11] D. Buskulic et al., Phys. Lett. **B313** (1993) 5099.
- [12] P. Abero et al., Z. Phys. **C62** (1994) 357.
- [13] H. Abramowicz, K. Charchula, A. Levy, Phys. Lett. **B269** (1991) 458.
- [14] M. Drees and K. Grassie,, Z. Phys. **C28** (1985) 451.
- [15] H. Hayashii et al., Phys. Lett. **B314** (1993) 149.
- [16] B. J. Kim et al., Phys. Lett. **B325** (1994) 248.
- [17] K. Muramatsu et al., Phys. Lett. **B332** (1994) 477.
- [18] M. Drees, M. Krämer, J. Zunft, and P. M. Zerwas, Phys. Lett. **B306** (1993) 371.
- [19] R. Enomoto et al., Phys. Rev. **D38** (1994) 1879.
- [20] R. Enomoto et al., Phys. Lett. **B328** (1994) 535.
- [21] T. Aso et al., KEK Preprint 95-19, Talk presented at Photon'95, April, 1995, Sheffield, U. K.
- [22] R. Enomoto et al., Phys. Lett. **B341** (1994) 238.
- [23] K. Hagiwara, M. Tanaka, I. Watanabe, and T. Izubuchi, Phys. Rev. **D51** (1995) 3197.
- [24] M. Iwasaki, E. Nakano and R. Enomoto, KEK Preprint 94-180, to be published in Nucl. Instrum. Meth. A.
- [25] M. Iwasaki et al., Phys. Lett. **B341** (1994) 99.
- [26] S. Uehara et al., Z. Phys. **C63** (1994) 213.
- [27] B. Andersson, G. Gustafson, T. Sjöstrand, Physica. Scripta. **Vol. 32** (1985) 574.

- [28] R. Enomoto et al., Phys. Lett. **B347** (1995) 179.
- [29] J. M. Butterworth, DESY 95-043.
- [30] I. Kronkvist and B. W. Kennedy, talk presented at Photon'95, April 1995, Sheffield, U. K.
- [31] R. Enomoto et al., submitted for publication.